Dalton Transactions

ROYAL SOCIETY OF CHEMISTRY

PAPER

View Article Online
View Journal

Cite this: DOI: 10.1039/d5dt02915e

Reservoir effect in bichromophoric Fe^{III} complexes with a methylene bridge

Lennart Schmitz,[a] Samira Dabelstein,[b] Miguel A. Argüello Cordero,[b] Lorena Fritsch,[a] Bastian Bracht,[a] Roland Schoch,[a] Hans Egold,[a] Jakob Steube,[a] Felix Fischer,[a] Stefan Lochbrunner[b] and Matthias Bauer *[a]

Received 5th December 2025,
Accepted 16th February 2026

DOI: 10.1039/d5dt02915e

rsc.li/dalton

Replacing noble metals in photocatalytic systems by their abundant counterparts to enhance sustainability aspects is the focus of current research. Iron is still a dream candidate despite the usually short lifetimes of photoactive states. The multichromophoric approach, where an organic chromophore with a long triplet lifetime acts as an excited state reservoir when connected to an iron complex, is a highly promising strategy that has gained attention recently. This effect cannot be realized by direct covalent connection of organic chromophores to the Fe^{III} complex $[Fe(ImPH)_2][PF_6]$ (HImPH = 1,1′-(1,3-phenylene)bis(3-methyl-1-imidazol-2-ylidene)) due to highly delocalized states enabling fast relaxation pathways. In this work, we present the effect of the shortest aliphatic chain bridge, *i.e.*, methylene, on the electronic state decoupling in complexes combining the base complex $[Fe(ImPH)_2][PF_6]$ with both phenyl and anthracenyl moieties as chromophoric entities. Chromophore connection to $[Fe(ImPH)_2][PF_6]$ was realized at the central phenyl ring and on the imidazole sides, resulting in four multichromophoric complexes. A thorough ground and excited state characterization was carried out in addition to extensive DFT calculations. The results clearly show an efficient decoupling utilizing the smallest possible space in a methylene bridge, realizing a reservoir effect for the anthracenyl-substituted complexes leading to excited state lifetimes beyond 5 ns.

Introduction

The replacement of precious metals like ruthenium and iridium with more abundant 3d transition metals in photoactive complexes is a highly active research field.[1–4] Iron is one of the dream candidates due to its abundance, but the realization of active state lifetimes that can potentially be used for photochemical applications requires creative approaches.[5–7]

The application of the reservoir effect, which has been known for around two decades in other transition metal complexes,[3,8,9] opens a new, promising method for tuning the lifetime of iron complexes.[6,7,10] It combines the advantages of organometallic and organic chromophores by integrating both units into one molecule.

Many organic chromophores show triplet excited states with long lifetimes but lack a large absorption cross section in the visible range and efficient intersystem crossing (ISC) from the optically excited singlet state to the triplet manifold.[11] Transition metal complexes, on the other hand, often undergo complete ISC and exhibit strong visible light absorption.[2] However, especially first-row transition metal complexes suffer from short-lived excited charge transfer (CT) states. Therefore, after optical excitation of the CT state on the organometallic part and subsequent ISC, the excited state population can be transferred to the triplet chromophore state ^{3}Chrom. When the excited state energies of the chromophore and the metal complex are similar, a reservoir effect in the form of an equilibrium between both states is possible.[8,12] The consequence is an extended metal-centred charge transfer state lifetime due to the long lifetime of the ^{3}Chrom state.[13]

In a previous study, a series of Fe^{III} complexes with different chromophores directly attached to a C^C^C ligand (**$[Fe(ImPChrom)_2][PF_6]$**, where HImPChrom = 1,1′-(5-(chromophore)-1,3-phenylene)bis(3-methyl-1-imidazol-2-ylidene), chromophore = phenyl, naphthyl, anthracenyl, and pyrenyl) was investigated.[14] While it was possible to tune the absorption cross section of the complex, a reservoir effect was not observed. In contrast to the initial idea, the chromophore significantly quenched the lifetime of the ligand-to-metal charge transfer state (^{2}LMCT). This effect is caused by strong electronic coupling between the organic chromophore and the iron complex in the excited state.

Recently, the importance of electronic decoupling in bichromophoric complexes was demonstrated by Wenger

[a]Faculty of Science, Chemistry Department and Center for Sustainable Systems Design, Paderborn University, 33098 Paderborn, Germany.
E-mail: bauerm@mail.uni-paderborn.de
[b]Institute of Physics and Department of Life, Light and Matter, University of Rostock, 18059 Rostock, Germany

et al.[3] They achieved decoupling by introducing a *meta*-substituted phenylene between the ImP ligand and the anthracenyl group. This led to an excited state lifetime of 1.4 ns for unmodified anthracenyl, which could be boosted to almost 100 ns by the introduction of a second anthracenyl moiety and excited state tuning by replacing anthracenyl with 9-cyanoanthracenylene, proving the viability of utilizing the reservoir effect in iron complexes. The scientific interest in this combination of the Fe photosensitizer (PS) with organic chromophores is underlined by a second recent publication by Troian-Gautier *et al.*, who utilized a different Fe(III) complex substituted with an anthracenyl chromophore.[6] While an equilibrium between the ^{2}LMCT and ^{3}Chrom states was not achieved, they observed mono-directional energy transfer into a dark ^{3}Chrom state with a lifetime of more than 10 μs.

In this work, we explore a novel decoupling approach by application of the smallest possible 'spacer' between the Fe^{III} base complex **C0** ($[Fe(ImP)_2][PF_6]$)[4] and the chromophoric phenyl and anthracenyl fragments in the form of a methylene bridge. This substitution is achieved at two positions of the base complex. By substitution in the backbone of the central phenylene, complexes analogous to the aforementioned $[Fe(ImPChrom)_2]^+$ complexes are obtained, further referred to as $[Fe(Im_2PPh)_2]^+$ and $[Fe(Im_2PAnt)_2]^+$ (see Scheme 2). A second set of complexes was realized by substitution of the *N*-imidazole methyl groups for methylene-chromophore groups, referred to as $[Fe((ImPh)_2P)_2]^+$ and $[Fe((ImAnt)_2P)_2]^+$ (see Scheme 1). As a result, an effective electronic decoupling between the iron complex and the chromophore could be achieved in the excited state and a reservoir effect could be observed *via* these simple methylene bridges.

Results

Synthesis

Four Fe^{III} complexes with methylene bridge connected chromophores were synthesized following two synthetic routes (see Schemes 1 and 2). Anthracenyl and phenyl chromophores were utilized. Anthracene exhibits a triplet energy of 1.84 eV,[15] slightly lower than the LMCT energy of the base complex **C0** (1.90 eV),[4] and should therefore be a suitable candidate to realize a reservoir effect. The phenyl chromophore is used for comparison as the reference chromophore with a non-matching triplet state energy (3.66 eV).[15]

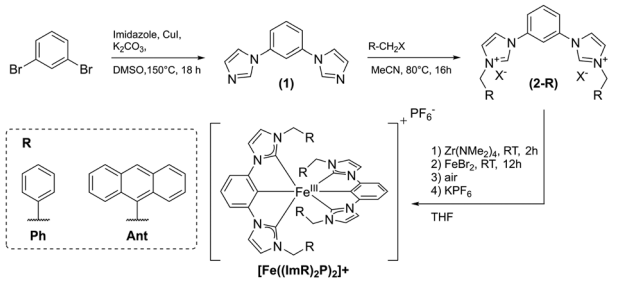

Scheme 1 Synthetic route for the complexes $[Fe((ImR)_2P)_2]^+$ from 1,3-dibromobenzene.

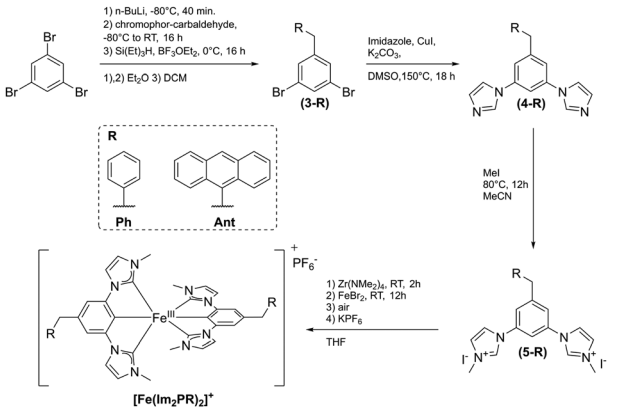

Scheme 2 Synthetic route for the synthesis of the complexes $[Fe(Im_2PR)_2]^+$ from 1,3,5-tribromobenzene.

The two complexes with modified imidazole groups (Scheme 1), with a total of four chromophores each, were obtained by first synthesizing **1** from 1,3-dibromobenzene using imidazole through an Ullmann-style coupling.[16] The imidazole moieties were then reacted with either bromotoluene or 9-(chloromethyl)anthracene to obtain **2-Ph** and **2-Ant**, respectively. By the application of a well-established synthetic route for cyclometalated iron complexes *via* an intermediate Zr-complex,[17] the desired complexes $[Fe((ImPh)_2P)_2]^+$ and $[Fe((ImAnt)_2P)_2]^+$ were obtained. After the synthesis, $[Fe((ImAnt)_2P)_2]^+$ was observed to decompose under irradiation, resulting in a free anthracene species (*cf.* the SI, Fig. S1). While this complicated the characterisation, it was still possible to obtain satisfactory results by utilizing fresh samples for each measurement.

The backbone-substituted complexes, with a total of 2 chromophores in the backbone, were obtained by a different synthetic approach (Scheme 2). The ligand precursors **3-R** were synthesized following a procedure reported by Young *et al.*[18] While this route was published for **3-Ph**, only minor modifications (see the SI) in the procedure were necessary for **3-Ant**.

First, 1,3,5-tribromobenzene was lithiated and subsequently reacted with either phenyl or anthracenyl carboxaldehyde. The resulting intermediate alcohols were reduced with triethylsilane in the presence of BF_3OEt_2 to obtain products **3-R**. These were then converted to the proligands following the previously shown route, where an Ullmann-style coupling was followed by alkylation with methyl iodide instead of the chromophore, methylene halides, to obtain **5-R**. In the final step, the $[Fe(Im2PPh)2]^+$ and $[Fe(Im2PAnt)2]^+$ complexes were obtained *via* the same complexation procedure as shown above.

Ground and excited state characterization

After several crystallization attempts, the obtained single crystals of these complexes were not suitable for the publication of crystallographic data, but we were able to prove connectivity of the backbone-substituted species (*cf.* the SI, Fig. S2). All com-

plexes were instead identified by a combination of HR mass spectroscopy, NMR analysis, and elemental analysis. The electronic ground and excited states were investigated using a wide array of analytical methods and *ab initio* calculations.

The chemical shifts in NMR spectroscopy serve as a first indicator for the success of electronic decoupling of the base complex and chromophore moieties. Since the investigated complexes are paramagnetic, a deviation alternating between negative and positive changes from the typical chemical shift in diamagnetic complexes is expected due to a continued electron polarization starting from the unpaired electron at the Fe^{III} centre.[19] This effect is shown in Fig. 1, which displays the deviation of the ^{13}C-NMR shifts in $[Fe(Im_2PPh)_2]^+$ from a typical value of 130 ppm for aromatic carbons.[20] The shifts are compared to those observed in the previously published $[Fe(ImP\text{-}Ph)_2]^+$.[14] The two complexes differ only in the bridging methylene group.

While the carbons located at the central ImP ligand (C1 to C3) show essentially equal shifts in both complexes, this trend clearly subsides after the first carbon of the attached phenylene (C5): C6 to C8 in the "spacerless" complex retain a significant deviation from the typical 130 ppm, showing the coupling of the phenyl group with the paramagnetic complex. In contrast, these carbons show shifts in the expected range for aromatic carbons in $[Fe(Im_2PPh)_2]^+$, indicating a missing influence of the unpaired electron on the Fe^{III}. Thus, an efficient electronic decoupling of the phenyl moiety from the central complex part is concluded. The strong deviation observed for the shift of C5 can be explained by hyperconjugation through the bridging methylene group. A similar trend is observed for $[Fe((ImPh)_2P)_2]^+$; however, this trend is less clear, since the paramagnetic effect on NMR resonances is generally lower in the imidazolyl groups (see SI Fig. S3). This electronic decoupling is also apparent for the anthracene-substituted complexes. Since the corresponding anthracene complex with a directly conjugated anthracene moiety in the backbone is already decoupled in the ground state due to a high dihedral angle that only planarizes upon excitation,[14] a similar comparison to that in Fig. 1 for $[Fe(Im_2PAnt)_2]^+$ is not possible.

To provide deeper insight into the underlying electronic structure of the complexes, DFT-optimized molecular geometries of the four complexes were obtained by predicting a distorted octahedral structure in the electronic ground state (^{2}GS) for all complexes. These calculated structures are in good agreement with the single-crystal XRD results we were able to obtain for $[Fe(Im_2PPh)_2]^+$ and $[Fe(Im_2PAnt)_2]^+$ (see Fig. S2). A closer examination of the spin density in the optimized ground state (see Fig. 2) reveals that spin polarization extends across the entire base complex, while the chromophores themselves exhibit almost no spin density. This observation agrees with the results obtained from NMR spectroscopy, which show little influence of the unpaired electron of the Fe^{III} centre on the chromophore. Consequently, the postulated decoupling of the chromophores from the central complex moiety is supported by the calculations, which is an important aspect for the realization of a reservoir effect.

The ground state oxidation and reduction potentials were analysed *via* cyclic voltammetry. The resulting voltammograms are shown in Fig. 3. All complexes show the same three redox processes as the unsubstituted base complex **C0**:[4,21] an $Fe^{III/IV}$ transition around 0 V, an $Fe^{II/III}$ transition below −1 V and a ligand oxidation around 1 V. While the iron redox processes are reversible, the oxidation of ligands exhibits only partial reversibility for the phenyl-substituted complexes and no reversibility for the anthracenyl-substituted complexes as previously observed for the directly substituted complexes.[14] Additionally, the anthracene containing complexes exhibit ligand oxidation at slightly smaller potentials, as is expected for larger

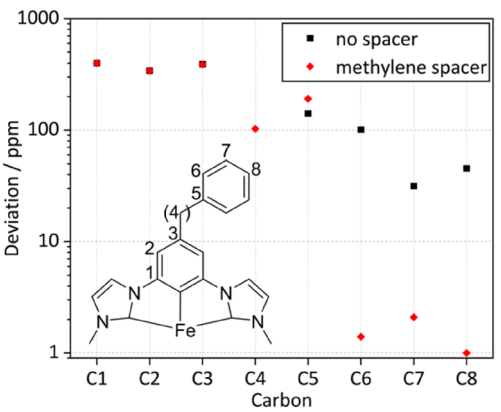

Fig. 1 Absolute deviation from the expected chemical shift in ^{13}C-NMR spectroscopy. The central phenyl carbons C1–C3 and backbone carbons C5–C7 of the two complexes $[Fe(ImP\text{-}Ph)_2]^+$ and $[Fe(Im_2PPh)_2]^+$ are referenced against a roughly expected value of 130 ppm. In addition, the bridging carbon C4 only present in $[Fe(Im_2PPh)_2]^+$ is depicted and referenced against 30 ppm.[20]

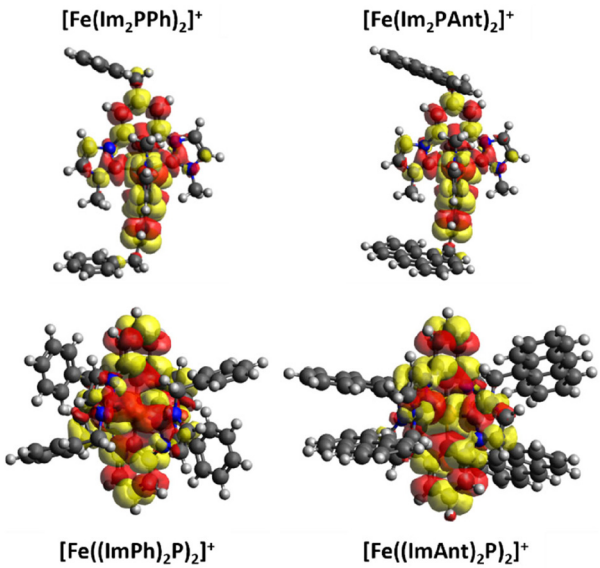

Fig. 2 Spin density plots of $[Fe(Im_2PPh)_2]^+$, $[Fe(Im_2PAnt)_2]^+$, $[Fe((ImPh)_2P)_2]^+$ and $[Fe((ImAnt)_2P)_2]^+$ (from left to right).

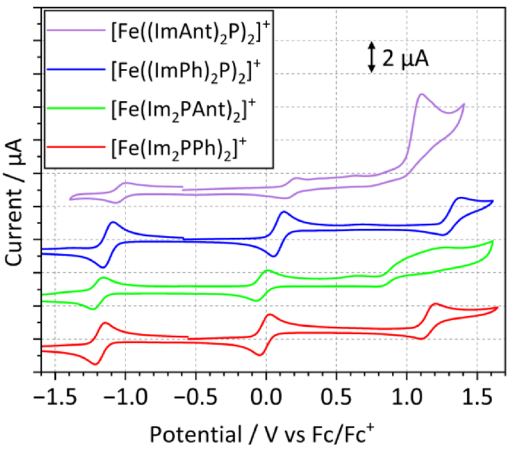

Fig. 3 Cyclic voltammograms of the four investigated complexes in MeCN with 0.1 M [nBu$_4$N][PF$_6$] at a scan rate of 0.1 V s^{-1}. The complexes were measured at a concentration of 1 mmol l^{-1}. The side-substituted anthracene complex was significantly less soluble and was measured at 0.3 mmol l^{-1}. To improve readability, the measured current was scaled by a factor of 1.5.

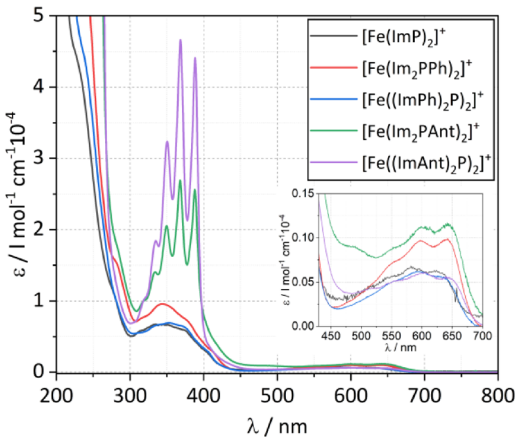

Fig. 4 UV-vis absorption spectra of all complexes and the base complex **C0** (c = 10^{-5} M) in MeCN.

π-systems, which are more suited to stabilizing the introduced positive charge. The oxidation of anthracene occurs at similar oxidation potentials.[22] The corresponding values are listed in Table 1.

The metal redox potentials seem to be primarily influenced by the substitution position. The backbone-substituted complexes show virtually identical oxidation/reduction potentials, whereas those of the side-substituted species are shifted to higher potentials. **[Fe((ImPh)$_2$P)$_2$]$^+$** shows potentials shifted by 0.1 V (Fe$^{III/IV}$) and 0.06 V (Fe$^{II/III}$) compared to **[Fe(Im$_2$PPh)$_2$]$^+$**. This effect is amplified by the anthracene substituent, where **[Fe((ImAnt)$_2$P)$_2$]$^+$** shows potentials shifted by 0.21 V (Fe$^{III/IV}$) and 0.16 V (Fe$^{II/III}$) compared to **[Fe(Im$_2$PAnt)$_2$]$^+$**. The origin of these counterintuitive shifts is not yet clear. However, similar results were found for an analogous Co(III) complex.[23]

Stationary absorption and emission spectra

The electrochemical properties provide insight into the electronic environment of the complexes, which also influences their optical behaviour. To further understand these effects, the electronic transitions were investigated *via* UV/vis and fluorescence spectroscopy. The near UV and visual range, as shown in Fig. 4, can be divided into three distinct absorption ranges, which can be assigned by comparison with similar previously published systems and TD-DFT calculations (*vide infra*).[4]

Below 300 nm, π–π*-transitions lead to strong absorption, especially for the anthracene-substituted complexes. Between 300 and 500 nm, mainly MLCT transitions are located, as was observed for similar complexes.[14] However, for the anthracenyl-substituted complexes, this absorption is masked by a strong characteristic absorption band corresponding to the singlet anthracene absorption.[24] This absorption band is just slightly shifted from the corresponding band in free anthracene since the methylene spacer largely prevents excited states involving both parts of the ligand (anthracenyl and bisimidazole phenylene). This is apparent when combining the base complex spectrum with the free anthracene spectrum multiplied by 2 or 4 depending on the number of chromophores in the complex, as shown in the SI (Fig. S4).

In addition to the literature comparison, vertical transitions of the optimized geometries in the UV/vis range were calculated using the B3LYP functional[25] and compared to the experimental spectra, supporting our band assignments. In Fig. 5, the spectra of the backbone-substituted complexes are shown, while those of the side-substituted complexes are shown in the SI (Fig. S15). Additionally, transition density analysis was performed to identify the involved orbitals in the different transitions. The calculated spectra of the complexes with phenyl substituents are in good agreement with the experimental data, while those of the anthracene-containing complexes are less well reproduced. This discrepancy is mainly attributed to the fact that TD-DFT is not taking vibronic progression into account, which is responsible for the typical absorption structure of anthracene.[26] The band in the range of 300–400 nm exhibits a mixed character. The most intense transition, centred around 340 nm for all complexes, is predominantly MLCT in nature involving acceptor orbitals, which mostly comprise the ImP ligand excluding the chromophores.

Table 1 Redox potentials of the investigated complexes in MeCN

	Fe$^{II/III}$ [V]	Fe$^{III/IV}$ [V]	Lig. oxidation [V]
[Fe(Im$_2$PPh)$_2$]$^+$	−1.18	−0.01	1.15
[Fe((ImPh)$_2$P)$_2$]$^+$	−1.12	0.09	1.32
[Fe(Im$_2$PAnt)$_2$]$^+$	−1.19	−0.04	0.87, 1.20[a]
[Fe((ImAnt)$_2$P)$_2$]$^+$	−1.03	0.17	1.09[b]
C0 (ref. 4)	−1.16	0.08	1.31[b]

[a] For **[Fe(Im$_2$PAnt)$_2$]$^+$**, a rather broad oxidation peak was observed, revealing two separate oxidation states in square wave voltammetry results listed here. [b] For the oxidation of ligands in the anthracene complexes, the anodic potential is listed.

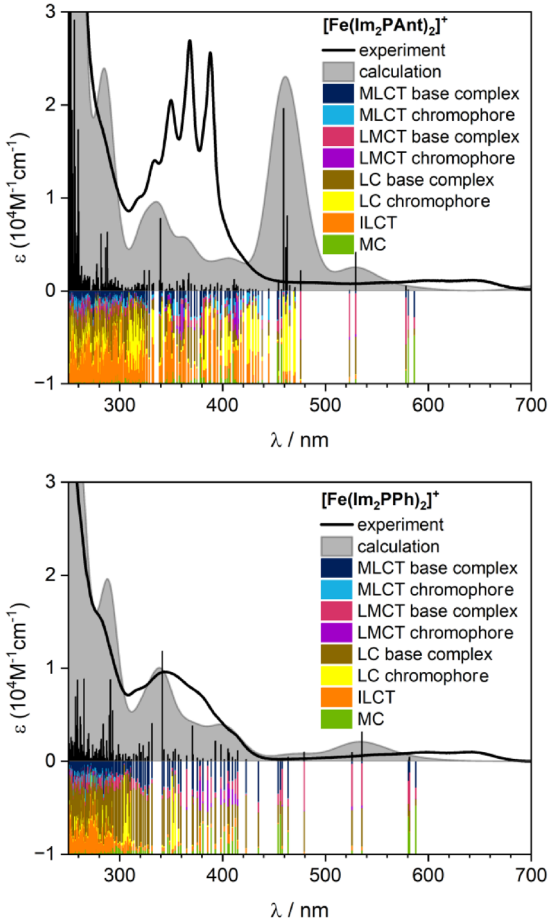

Fig. 5 Experimental and TD-DFT-calculated UV-vis spectra (broadened with a full-width at half maximum (FWHM) of 2000 cm^{-1}) of **[Fe(Im$_2$PPh)$_2$]$^+$** and **[Fe(Im$_2$PAnt)$_2$]$^+$**. LC refers to electronic transitions where the charge remains localized within the same part of the ligand (base complex ligand or chromophore), whereas ILCT (intra ligand charge transfer) describes charge transfer between different regions within the same ligand.

Additionally, ligand-centred (LC) transitions located within the ImP framework contribute to this band. In the anthracenyl-substituted systems, a significant portion of the absorption also arises from purely chromophore-based LC transitions. While these transitions are predicted by the calculations at around 460 nm, they can be associated with the experimentally observed band in the 300–400 nm range, suggesting a slight underestimation of their energy in the computational results.

The low-energy band at around 600–650 nm is identified as a ligand-to-metal charge transfer (LMCT) band in the central complex moiety, consistent with the experimental observations discussed earlier and calculations for similar systems.[4,14] For the anthracene-containing complexes, the calculations predict that this band also exhibits a slight anthracene-based LMCT character. Due to the increased number of chromophores, this character is especially visible in **[Fe((ImAnt)$_2$P)$_2$]$^+$**.

The UV/Vis calculations only account for spin-allowed excitation. However, indirect insights into the energetic alignment can be obtained. For the anthracenyl-containing complexes, chromophore-based transitions appear close in energy to the LMCT band (600–650 nm). This suggests that the corresponding chromophore state is also in this range, facilitating a reservoir effect. In contrast, the phenyl-substituted complexes exhibit chromophore-based transitions at much higher energies, implying that the energy of the triplet states is too high to efficiently interact with the LMCT state. Further support comes here from the calculated ground state orbital energies (Fig. 6), which reveal that the energy gap between the HOMO and the LUMO of the anthracene-based chromophore is comparable to that of the LUMO of the base complex ligand and the HOMO of the metal.

The much stronger experimental absorptivity of **[Fe((ImAnt)$_2$P)$_2$]$^+$** (ε_{368nm} = 4.5 × 10^4 M^{-1} cm^{-1}) compared to **[Fe(Im$_2$PAnt)$_2$]$^+$** (ε_{368nm} = 2.7 × 10^4 M^{-1} cm^{-1}) is due to the increased number of organic chromophores (four instead of two). The characteristic anthracene bands are only slightly shifted compared to free anthracene,[27] indicating an effective electronic decoupling of the chromophore from the complex. The MLCT bands observed in the phenyl-substituted complexes are also not notably shifted, with only a slight enhancement in intensity in the case of **[Fe(Im$_2$PPh)$_2$]$^+$** compared to **C0**. This observation further underlines the limited influence of the methylene-bridged chromophore on MLCT transitions. The bands above 500 nm are dominated by LMCT transitions. Here, the same trends as for the MLCT bands are obvious. While the side-substituted complexes show no changes in extinction coefficients or band positions, the backbone-substituted complexes show virtually no changes in extinction coefficients. This contrasts with the complexes that contain a chromophore directly linked to the iron complex. They show a larger influence of the chromophore backbones on the MLCT and LMCT states.[14] In conclusion, the absorption properties of the decoupled complexes are less favourable when compared to direct connection and conjugation. However, this reduced interaction is an expected side effect of the desired decoupling, considered as a prerequisite for the reservoir effect.

Efficient decoupling of the chromophores from the complexes is also observable in stationary emission spectroscopy. For this, all complexes were excited at 350 nm (MLCT range).

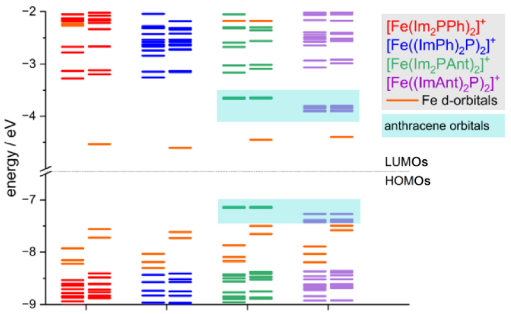

Fig. 6 DFT (B3LYP) calculated ground state orbital energies of all four complexes.

As observed for similar complexes before, this leads to an emission from the LMCT state above 650 nm following Kasha's Rule.[28] This relaxation from ^{2}MLCT to ^{2}LMCT was previously reported and investigated in more depth after an originally reported dual emission was shown to be erroneous. The lifetime of this ^{2}MLCT state for **C0** is smaller than 10 ps and was not investigated for the systems presented here.[29] The high extinction coefficients in this range enable a stronger emission signal. To confirm the nature of the present emission, additional emission spectra after excitation at 600 nm (LMCT range) leading to the same emission bands are presented in the SI (Fig. S5). All complexes show a similar LMCT emission to **C0**, with maxima between 700 and 750 nm, as shown in Fig. 7.

Consequently, even after optical excitation, the electronically excited states remain largely decoupled due to the bridging methylene group. Therefore, energetically low-lying mixed states are prevented, which would result in a fast non-radiative decay, as is the case for the complexes with a directly substituted chromophore.[14] As a reminder, among such complexes with direct connection between the iron complex and chromophores, only those functionalised with phenyl and naphthalene showed a comparable LMCT emission to **C0** due to their high triplet energy. However, pyrene- and anthracene-functionalised complexes resulted in a significantly weakened and redshifted LMCT emission due to the formation of a "superligand" LMCT state, delocalized over the whole complex.

Instead, the emission of the anthracene-substituted complexes in this study is only weakened, as is apparent from the non-normalized emission spectra in the SI (Fig. S5). To a lesser extent, the side-substituted complexes exhibit weaker emission than their backbone-substituted counterparts, leading to the emission intensity order $\mathbf{[Fe(Im_2PPh)_2]^+}$ > $\mathbf{[Fe((ImPh)_2P)_2]^+}$ > $\mathbf{[Fe(Im_2PAnt)_2]^+}$ > $\mathbf{[Fe((ImAnt)_2P)_2]^+}$. Additionally, the side-substituted complexes have slightly redshifted emission maxima, which may relate to the shifted potentials observed in cyclic voltammetry (*vide supra*).

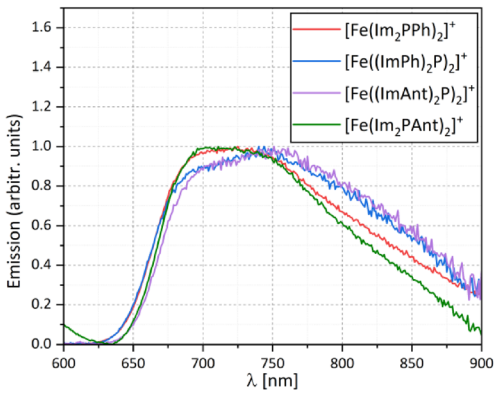

Fig. 7 Emission spectra of all investigated complexes excited at 350 nm. The emission spectra are normalized for improved comparability. All spectra were measured in MeCN (10^{-5} M).

The anthracene-substituted compounds also exhibit singlet anthracene emission, as shown in SI Fig. S5. As stated in a previous publication, a likely explanation for this emission is a minor impurity of free anthracene that leads to a strong effect on the emission spectra due to the high quantum yield of anthracene.[14] Because of its very low concentration and the wavelength of the emission, we do not expect this to interfere with any other measurements done in this study.

Since the emission intensity of the reservoir-enabled complexes relies on thermal energy for a back transfer to the LMCT state, all complexes were investigated in low-temperature emission spectroscopy (see the SI, Fig. S6). Both phenyl complexes exhibit emission significantly increased by a factor of 10 when cooled to 77 K with two maxima at around 675 nm and 740 nm, due to the vibronic fine structure of the LMCT state. While an increase in emission intensity is also apparent for $\mathbf{[Fe(Im_2PAnt)_2]^+}$, the effect is weaker by a factor of 5 compared to room temperature measurements. This weaker emission intensity enhancement is due to the back transfer from the ^{3}Chrom state to the ^{2}LMCT state being inhibited at low temperatures. Since many excited electrons never enter the ^{3}Chrom state and instead relax into the ground state immediately, the emission is still enhanced, albeit to a lesser extent. This increase in emission intensity is even weaker for $\mathbf{[Fe((ImAnt)_2P)_2]^+}$ by a factor of about 2, which is presumably the result of the increased number of anthracene units, accelerating the quenching of the LMCT state. Due to the generally weak emission of these compounds, an increasing baseline with lower temperatures and scattering from the frozen butyronitrile affect these measurements significantly, as can be seen in Fig. S6 in the SI. However, the general trend of an increasing emission intensity is still apparent.

Time-resolved emission measurements

The temporal evolution of the LMCT emission was studied using a streak camera and TCSPC measurements for all four complexes. The results obtained for $\mathbf{[Fe(Im_2PAnt)_2]^+}$ are shown in Fig. 8, and all other data on the emission dynamics are presented in the SI (Fig. S6 and S7). For $\mathbf{[Fe(Im_2PPh)_2]^+}$ and $\mathbf{[Fe((ImPh)_2P)_2]^+}$ excited in the LMCT absorption band at 600 nm, a monoexponential decay of the fluorescence with a time constant of 0.19 and 0.20 ns, respectively, is found. These values are close to the LMCT lifetime of the base complex **C0** (0.24 ns), pointing to a similar relaxation cascade.

Conversely, the anthracene-functionalized complexes show very distinct photodynamics. The emission is weaker (Fig. S7) and exhibits time zero contributions caused by scattering of the excitation light. After a pronounced signal drop within the experimental time resolution, a part of the LMCT emission remains and decays monoexponentially with a time constant of 5.3 ns. These findings are shown in the bottom graph of Fig. 8 by the amplitude spectra of the fast and monoexponentially decaying component, which are obtained by a global lifetime analysis described below. The spectrum of the 5.3 ns component resembles the stationary emission spectrum very well, strongly indicating that it is due to emission from the

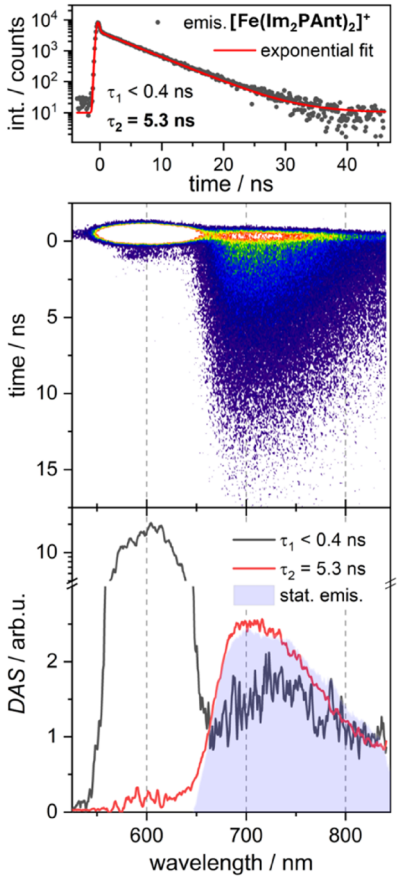

Fig. 8 Time-resolved emission of $[Fe(Im_2PAnt)_2]^+$ dissolved in MeCN after optical excitation at 600 nm. Top: time trace of the spectrally integrated emission intensity (int. in total counts, black dots) together with a double exponential fit. The short time constant of the fit is below the time resolution of the measurement, and the corresponding signal contribution can be regarded as practically instantaneous. Middle: two-dimensional plot of the time-resolved emission intensity. Bottom: decay-associated amplitude spectra (DAS) resulting from a global lifetime analysis of the dataset with two exponential decay components. For comparison, the stationary emission spectrum is shown (grey area). The *y*-axis has a logarithmic scale above a break at 3 arbitrary units (arb. u.) to enable a plot including the high-intensity areas.

LMCT state. If the emission originated from anthracene, the characteristic vibrational structure of the anthracene fluorescence would be expected at shorter wavelengths.[30] Thus, a significant contribution of anthracene fluorescence can be excluded. The fast component is dominated by scattered excitation light around 600 nm.

The results show that the lifetime of the excited state population is extended to several nanoseconds in the anthracenyl-substituted complex $[Fe(Im_2PAnt)_2]^+$. However, most of it does not reside in the LMCT state, since the LMCT emission is not very intense. This observation indicates that another state operates as a reservoir for the excited state population. The local triplet state of the chromophore is a natural candidate, as it has a suitable energy and a very long lifetime. This is further investigated in the transient absorption studies (*vide infra*). Time-resolved emission was measured using time-correlated single photon counting (TCSPC), which exhibits a higher dynamic range, but a reduced spectral resolution compared to streak camera measurements, reproduced the results obtained with the latter, see Fig. S9 in the SI.

The emission of $[Fe((ImAnt)_2P)_2]^+$ shows a very similar behaviour to that of $[Fe(Im_2PAnt)_2]^+$, see Fig. S6 and S7 for the corresponding measurements with the streak camera and their evaluation. Again, the emission at time zero is dominated by scattered excitation light and drops immediately after the optical excitation. Thereafter, weak emission from the LMCT state with a lifetime of 4.4 ns is observed. Interestingly, a similar system with anthracene as the reservoir was recently reported by Wenger *et al.* with a lifetime of 1.4 ns.[7] Instead of a methylene bridge, a *meta*-substituted phenyl spacer was utilized to achieve electronic decoupling. Additionally, chromophores with lower triplet state energies were utilized to match (9-phenyl anthracene at 5.2 ns) or exceed (9-cyano-anthracene at 45 ns for two chromophores and 98 ns for four chromophores) the lifetimes reported here.

Ultrafast transient absorption measurements

To investigate the photo-induced dynamics of the complexes with higher time resolution and to characterize the nature of the reservoir state, ultrafast transient absorption (TA) measurements were conducted. The phenyl-functionalized complexes exhibit similar TA signatures and dynamics to those of the base complex $[Fe(ImP)_2]^+$. Therefore, only the results for $[Fe(Im_2PPh)_2]^+$ are presented here, while those for $[Fe((ImPh)_2P)_2]^+$ are shown in the SI (Fig. S11). The TA spectra, as shown in Fig. 9A, are dominated by an excited state absorption (ESA) signal, representing the absorption of the excited states. Similar to **C0**,[4] the ESA signal builds up with the experimental time resolution and decays within a few hundred picoseconds. Due to the high concentration necessary for excitation in the LMCT band and the resulting strong sample absorption in the near ultraviolet (UV), it was not possible to record TA signals in the UV region. Therefore, only a part of the ESA band in the visible spectra could be studied. The ESA dominates the TA signal and covers the ground state bleach (GSB). In Fig. 9C, the spectral shape and position of the GSB are indicated in violet based on the stationary absorption spectra. The TA data $\Delta OD(\lambda,t)$ were globally analysed by fitting a sum of exponential decay components to the transient spectra following the function in section 7 in the SI.

An overview of the time constants obtained from this global lifetime analysis (GLA) can be found in Table 2, while the DAS are shown in the corresponding figures. For both phenyl-substituted complexes, two time constants were necessary to describe the evolution of the TA spectra, with one time constant being effectively infinite. In both cases, the contributions associated with the infinite time constant were minimal and are assumed to be artifacts of the measurements. The shorter time constants correspond to the LMCT lifetimes and were determined as 190 ps for $[Fe(Im_2PPh)_2]^+$ and 180 ps for $[Fe((ImPh)_2P)_2]^+$. The corresponding decay associated spectra

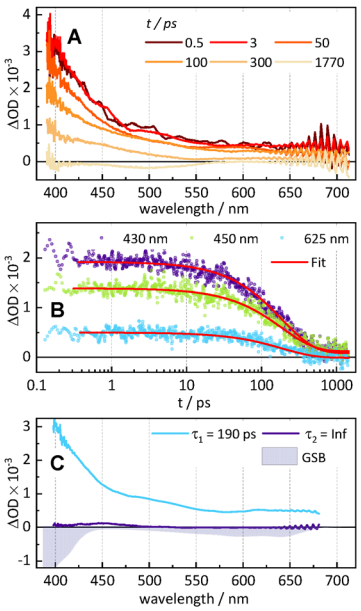

Fig. 9 (A) TA spectra of $[Fe(Im_2PPh)_2]^+$ in MeCN at different times *t* after optical excitation at 600 nm. (B) Time traces (dots) at the specified probe wavelengths together with respective fit curves resulting from the GLA (red solid line). (C) DAS obtained by GLA and labelled with the respective time constants. The dynamics are well described by a mono-exponential decay with a time constant of τ_1 = 190 ps. A further, long-lived component modelled by a decay with an infinite time constant τ_2 = inf was used to account for tiny offsets at long delay times. The component is at all wavelengths practically zero and within the experimental accuracy insignificant.

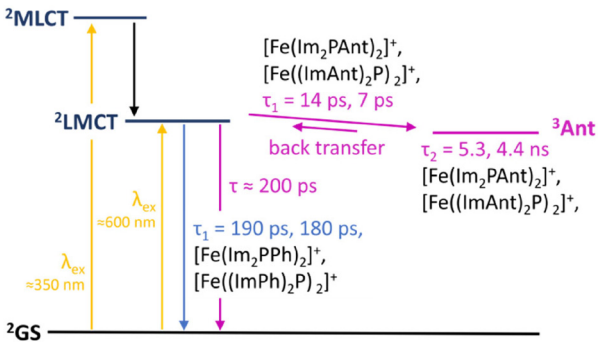

Scheme 3 Jablonski diagram describing the relaxation to the ground state after optical excitation into the ^{2}MLCT or ^{2}LMCT state. Decay steps of $[Fe(Im_2PPh)_2]^+$ and $[Fe((ImPh)_2P)_2]^+$ are shown in blue and decay processes of $[Fe(Im_2PAnt)_2]^+$ and $[Fe((ImAnt)_2P)_2]^+$ are shown in purple. Additional radiationless decay processes were obscured for clarity.

(DAS) are shown in Fig. 9C and Fig. S11C in the SI. The associated Jablonski diagram, see Scheme 3, illustrates that the complexes are excited from the ground state into the ^{2}LMCT state.

Excitation of the ^{2}MLCT band leads to population of the same state through internal conversion, as is evident from the same emission occurring after excitation of either band. The LMCT state decays directly back into the ground state with a lifetime given by the time constant τ_1.

This reduction in lifetime may be due to steric effects induced by different geometries ($[Fe((ImPh)_2P)_2]^+$) or electron pushing effects of the methylene spacer ($[Fe(Im_2PPh)_2]^+$). This difference is apparent, albeit small, when comparing the crystal structures of **C0** with the optimized geometries of these compounds in Table 3.

Next, the TA spectra of the complexes with anthracene as the substituent were analysed. Both complexes, $[Fe(Im_2PAnt)_2]^+$ and $[Fe((ImAnt)_2P)_2]^+$, exhibit similar dynamics, which differ from those of the basic and the phenyl-substituted complexes. As before, only the results for $[Fe(Im_2PAnt)_2]^+$ are presented here, while those for $[Fe((ImAnt)_2P)_2]^+$ are presented in the SI (Fig. S13A). After optical excitation, the TA spectra are dominated by a broad ESA band (Fig. 10A), similar to those of the other complexes, covering the ground state bleach. As before, the spectral shape and position of the GSB is indicated in grey based on the stationary absorption spectrum. However, after a few picoseconds, a new, narrow band with a sharp maximum around 425 nm emerges. This band results from the local $^3\pi\pi^*$ state of anthracene, as evidenced by a comparison with the triplet–triplet absorption of dissolved anthracene,[31] as well as with the transient spectra of an anthracene-functionalized ruthenium complex.[32] At the same time, the initial ESA contributions in the visible range disappear. The remaining ESA signal is highly persistent, with a lifetime exceeding the maximum delay time of 1.8 ns accessible with the present setup. Additionally, the TA spectra of the samples display two isosbestic points. For $[Fe(Im_2PAnt)_2]^+$, the isosbestic points are located at approximately 415 nm and 430 nm, while for $[Fe((ImAnt)_2P)_2]^+$, they are at approximately 415 nm and 435 nm. These isosbestic points suggest a straightforward population transfer without intermediate steps. To exclude other possible processes, we compared our results with the TA signature of singlet anthracene[33] and examined the stationary absorption spectra of the anthracene cation and anion.[34] This analysis allows both the population of the electronically excited singlet state of anthracene and any significant charge transfer to or from anthracene to be ruled out. Thus, the excited state population is at longer delay times in

Table 2 Time constants obtained by GLA of the TA data

	C0 (ref. 4)	$[Fe(Im_2PPh)_2]^+$	$[Fe((ImPh)_2P)_2]^+$	$[Fe(Im_2PAnt)_2]^+$	$[Fe((ImAnt)_2P)_2]^+$
τ_1	240 ps	190 ps	180 ps	14 ps	8 ps
τ_2	—	—	—	5.3[a] ns*	4.4[a] ns

[a] Time constant obtained from streak camera measurements.

Table 3 Relevant structural parameters for **C0** (crystal structure) and the investigated phenyl complexes (calculated structure)

Compound	**C0** (ref. 21)	$[Fe(Im_2PPh)_2]^+$	$[Fe((ImPh)_2P)_2]^+$
Fe–C_{phenyl} mean distance (Å)	1.948(3)	1.94	1.93
Fe–$C_{imidazole}$ mean distance (Å)	1.982(3)	2.01	2.00
Mean bite angle (°)	155.36(15)	156.0	156.5

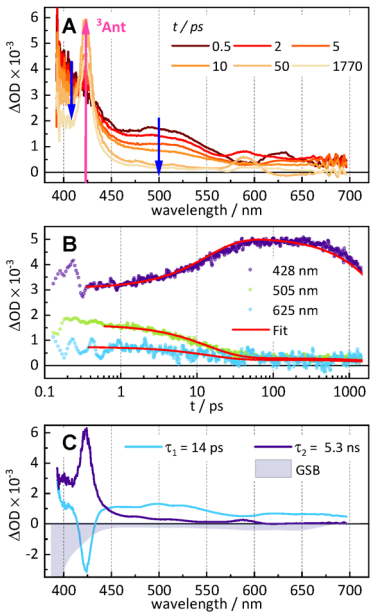

Fig. 10 (A) TA spectra of $[Fe(Im_2PAnt)_2]^+$ dissolved in MeCN at different times after optical excitation at 600 nm. (B) Time traces (dots) at the specified probe wavelengths together with respective fit curves resulting from the GLA (red solid line). (C) DAS obtained by GLA and labelled with the respective time constants. The dynamics is well described by a double exponential decay with time constants τ_1 = 14 ps and τ_2 = 5.3 ns.

the triplet state of the anthracene unit. Furthermore, we compared the TA spectrum of $[Fe(Im_2PAnt)_2]^+$ at 0.5 ps with the TA spectra of the corresponding "spacerless" complex $[Fe(ImP\text{-}Ant)_2]^+$ and the base complex **C0** at the same delay time, see Fig. S14. The data for the corresponding "spacerless" complex and the base complex **C0** were adapted from our previous publication.[14] The early TA signatures of all three complexes are very similar, supporting the conclusion that the LMCT state is initially populated upon photoexcitation of $[Fe(Im_2PAnt)_2]^+$. The TA data of the anthracene complexes were fitted with two exponential decay components, as shown in Fig. 10C. The shorter time constant τ_1 is associated with the rise of the narrow ESA band at 425 nm, which is evident from the fact that the corresponding DAS (blue) contains an inverted image of the narrow ESA band. Consequently, this component describes the population transfer from the ^{2}LMCT state to the local anthracene triplet state ^{3}Ant. In the case of $[Fe(Im_2PAnt)_2]^+$, the shorter time constant τ_1 amounts to 14 ps and for $[Fe((ImAnt)_2P)_2]^+$, it amounts to 8 ps. Therefore, the population transfer occurs twice as fast for the $[Fe((ImAnt)_2P)_2]^+$ complex with four anthracene units compared to the $[Fe(Im_2PAnt)_2]^+$ complex with only two anthracene units. This behaviour suggests that the transfer rate per anthracene unit is similar in both complexes and the faster dynamics of $[Fe((ImAnt)_2P)_2]^+$ are simply a result of the increased number of transfer acceptors and channels. However, this proportional relationship between the number of chromophores and the lifetime is not true for the LMCT emission lifetimes, which are similar for two ($[Fe(Im_2PAnt)_2]^+$) and four ($[Fe((ImAnt)_2P)_2]^+$) chromophore units. The apparent trend may therefore just be a coincidence. The DAS of the time constant τ_2 reflects the decay of the local anthracene triplet state on a timescale in the order of a few nanoseconds. Therefore, the time window of 1.8 ns accessible with the present setup is exceeded. Consequently, the time constant τ_2 cannot be determined accurately from the TA data. However, the time should be equal to the lifetime of the luminescence determined by the time-resolved emission experiments (see above). Indeed, fixing τ_2 to the values of 5.3 ns and 4.4 ns for $[Fe(Im_2PAnt)_2]^+$ and $[Fe((ImAnt)_2P)_2]^+$, respectively, in the GLA leads to excellent agreement between fits and data. Thus, the long-lived TA component is fully consistent with the luminescence behaviour of the complexes.

The light-induced dynamics of the anthracene-functionalized complexes is shown by pink arrows in the Jablonski diagram shown in Scheme 3. The anthracene complexes are excited from the ground into the ^{2}LMCT state, as is the case for the phenyl-substituted complexes. From there, a population transfer occurs with the time constant τ_1 to the local ^{3}Ant state, which then decays back to the ground state with the time constant τ_2. Thus, the excited state population is stored for several nanoseconds in the local triplet state of the anthracene substituents and a reservoir effect is achieved. The triplet lifetime of anthracene in solution is many orders of magnitude larger than τ_2.[35] In the complex, however, the ^{3}Ant state is depopulated by a weak back transfer of the population to the ^{2}LMCT state, which is also responsible for the observed fluorescence. The intrinsic lifetime of the ^{2}LMCT state should be on the order of 200 ps, comparable to those of the base and phenyl-substituted complexes.

Conclusion

In this work, four multichromophoric Fe^{III} complexes based on the previously published base complex **C0** ($[Fe(ImP)_2]^+$) were synthesized and investigated.[4] To potentially enable a reservoir effect, a methylene bridge as the smallest possible decoupling unit was installed between the central iron complex and the

organic chromophore functionalities.[14] The ImP framework was modified both in the backbone of the central phenylene and at the imidazole *N*-alkyl position. Anthracene was chosen as the chromophore with a triplet energy nearly matching that of the LMCT state of **C0**,[24] while the phenyl substituent serves as a reference with a chromophore energy being very different from the LMCT state. The electronic ground states and the excited state dynamics were investigated by experimental methods, supported by (TD-)DFT calculations.

The phenyl-substituted complexes $[Fe(Im_2PPh)_2]^+$ and $[Fe((ImPh)_2P)_2]^+$ show the same photodynamics as those of previously published complexes with emission lifetimes of about 200 ps.[14] In contrast, the anthracenyl-substituted complexes $[Fe(Im_2PAnt)_2]^+$ and $[Fe((ImAnt)_2P)_2]^+$ exhibit lifetimes that extend beyond 5 ns. This lifetime is associated with the population of the ^{3}Chrom state, which was confirmed by transient absorption spectroscopy. However, repopulation of the LMCT state is also necessary for the reservoir effect.[6] This aspect was confirmed by time-resolved emission spectroscopy, which revealed ns lifetimes of the excited state consistent with the TA results. Thus, a reservoir effect could be realized even with the spatially small methylene bridge, which allows an effective electronic decoupling between the iron complex part and the organic chromophore. In turn, this further confirms that both a considerable original CT state lifetime plus an electronic decoupling of the metal complex and the organic chromophore are mandatory to achieve a detectable reservoir effect.

Author contributions

L. S. and B. B. carried out the synthesis of the compounds. L. S., B. B. and H. E. carried out the characterisation of the compounds. L. S carried out the steady-state photophysical measurements, as well as the electrochemical and TCSPC measurements. S. D., M. A. C. and S. L. carried out the time-resolved measurements *via* transient absorption spectroscopy and streak camera measurements and analysed the data. L. F. carried out quantum chemical calculations. R. S. recorded and analysed the single-crystal X-ray diffraction data. L. S. drafted the manuscript together with S. D., M. A. C., L. F. and J. S. All authors read and commented on the manuscript. M. B. carried out conceptualization, supervised the project and contributed to writing the manuscript. F. F. supervised and contributed to the revision process of the manuscript.

Conflicts of interest

There are no conflicts to declare.

Data availability

Data supporting this article have been included in the supplementary information (SI). Supplementary information: detailed synthetic procedures, available single-crystal X-ray diffraction data, NMR spectra and additional paramagnetic NMR investigations, additional steady-state absorption and emission data, additional time-resolved emission data, additional TD-DFT data, and mass spectroscopy data. See DOI: https://doi.org/10.1039/d5dt02915e.

Data used in this publication are available at Zenodot (https://doi.org/10.5281/zenodo.18609881).

Acknowledgements

L. S. and L. F. thank the Fonds der Chemischen Industrie for a Kekulé grant. M. B. gratefully acknowledges financial support through the priority program SPP 2102 from the German Science Foundation DFG (BA 4467/7-2) and within the frame of project BA 4467/10-1. S. L. gratefully acknowledges financial support through SPP 2102 (LO 714/11-2) and GRK 2943 'Spectroscopic Tools for Challenging Reduction Reactions: Catalytic Coupling of CO2', project no. 507189291. S. L. further acknowledges funding from SFB 1477 'Light–Matter Interactions at Interfaces'. The grant of computer time at the Paderborn Center for Parallel Computing PC^2 is acknowledged.

References

1 (*a*) O. S. Wenger, *Chem. – Eur. J.*, 2019, **25**, 6043–6052; (*b*) P. Dierks, Y. Vukadinovic and M. Bauer, *Inorg. Chem. Front.*, 2022, **9**, 206–220; (*c*) A. Ghosh, J. T. Yarranton and J. K. McCusker, *Nat. Chem.*, 2024, **16**, 1665–1672; (*d*) M. Pastore, S. Caramori and P. C. Gros, *Acc. Chem. Res.*, 2024, **57**, 439–449.

2 C. Förster and K. Heinze, *Chem. Soc. Rev.*, 2020, **49**, 1057–1070.

3 C. Wegeberg and O. S. Wenger, *Dalton Trans.*, 2022, **51**, 1297–1302.

4 J. Steube, A. Kruse, O. S. Bokareva, T. Reuter, S. Demeshko, R. Schoch, M. A. Argüello Cordero, A. Krishna, S. Hohloch, F. Meyer, K. Heinze, O. Kühn, S. Lochbrunner and M. Bauer, *Nat. Chem.*, 2023, **15**, 468–474.

5 (*a*) W. Leis, M. A. Argüello Cordero, S. Lochbrunner, H. Schubert and A. Berkefeld, *J. Am. Chem. Soc.*, 2022, **144**, 1169–1173; (*b*) P. Chábera, K. S. Kjaer, O. Prakash, A. Honarfar, Y. Liu, L. A. Fredin, T. C. B. Harlang, S. Lidin, J. Uhlig, V. Sundström, R. Lomoth, P. Persson and K. Wärnmark, *J. Phys. Chem. Lett.*, 2018, **9**, 459–463; (*c*) A. R. Marri, B. Marekha, T. Penfold, S. Haacke and P. C. Gros, *Inorg. Chem. Front.*, 2022, **10**, 118–126.

6 F. Glaser, S. de Kreijger and L. Troian-Gautier, *J. Am. Chem. Soc.*, 2025, **147**, 8559–8567.

7 J. Wellauer, B. Pfund, I. Becker, F. Meyer, A. Prescimone and O. S. Wenger, *J. Am. Chem. Soc.*, 2025, **147**, 8760–8768.

8 D. S. Tyson and F. N. Castellano, *J. Phys. Chem. A*, 1999, **103**, 10955–10960.

9 A. J. Howarth, M. B. Majewski and M. O. Wolf, *Coord. Chem. Rev.*, 2015, **282–283**, 139–149.
10 (*a*) P. Dierks, A. Päpcke, O. S. Bokareva, B. Altenburger, T. Reuter, K. Heinze, O. Kühn, S. Lochbrunner and M. Bauer, *Inorg. Chem.*, 2020, **59**, 14746–14761; (*b*) S. Campagna, S. Genovese, A. Cancelliere, A. Arrigo and F. Puntoriero, *Fe (III) complexes with prolonged luminescence lifetimes and symmetry-breaking charge separation*, Preprint, 2024.
11 B. Valeur and M. N. Berberan-Santos, *Molecular Fluorescence. Principles and Applications*, Wiley-VCH, Weinheim, 2012.
12 A. F. Morales, G. Accorsi, N. Armaroli, F. Barigelletti, S. J. A. Pope and M. D. Ward, *Inorg. Chem.*, 2002, **41**, 6711–6719.
13 D. S. Tyson, J. Bialecki and F. N. Castellano, *Chem. Commun.*, 2000, 2355–2356.
14 L. Schmitz, M. A. Argüello Cordero, M. J. Al-Marri, R. Schoch, H. Egold, A. Neuba, J. Steube, B. Bracht, O. S. Bokareva, S. Lochbrunner and M. Bauer, *Inorg. Chem.*, 2025, **64**, 14101–14117.
15 M. Montalti, J. Michl and V. Balzani, *Handbook of photochemistry*, Taylor & Francis, Boca Raton, 3rd edn, 2006.
16 C. Li, C. Gao, J. Lan, J. You and G. Gao, *Org. Biomol. Chem.*, 2014, **12**, 9524–9527.
17 S. W. Reilly, C. E. Webster, T. K. Hollis and H. U. Valle, *Dalton Trans.*, 2016, **45**, 2823–2828.
18 L. Zhuang, J. S. Wai, M. W. Embrey, T. E. Fisher, M. S. Egbertson, L. S. Payne, J. P. Guare, J. P. Vacca, D. J. Hazuda, P. J. Felock, A. L. Wolfe, K. A. Stillmock, M. V. Witmer, G. Moyer, W. A. Schleif, L. J. Gabryelski, Y. M. Leonard, J. J. Lynch, S. R. Michelson and S. D. Young, *J. Med. Chem.*, 2003, **46**, 453–456.
19 M. Enders, *Assigning and Understanding NMR Shifts of Paramagnetic Metal Complexes*, Wiley-VCH, Weinheim, 1st edn, 2011.
20 H. Günther, *NMR Spectroscopy. Basic Principles, Concepts, and Applications in Chemistry*, Wiley-VCH, Weinheim, 3rd edn, 2013.
21 J. Steube, L. Fritsch, A. Kruse, O. S. Bokareva, S. Demeshko, H. Elgabarty, R. Schoch, M. Alaraby, H. Egold, B. Bracht, L. Schmitz, S. Hohloch, T. D. Kühne, F. Meyer, O. Kühn, S. Lochbrunner and M. Bauer, *Inorg. Chem.*, 2024, **63**, 16964–16980.
22 C. A. Paddon, C. E. Banks, I. G. Davies and R. G. Compton, *Ultrason. Sonochem.*, 2006, **13**, 126–132.
23 A. Krishna, L. Fritsch, J. Steube, M. A. Argüello Cordero, R. Schoch, A. Neuba, S. Lochbrunner and M. Bauer, *Inorg. Chem.*, 2025, **64**, 1401–1409.
24 S. L. Murov, I. Carmichael and G. L. Hug, *Handbook of photochemistry*, Marcel Dekker, New York, 2nd edn, 1993.
25 A. D. Becke, *J. Chem. Phys.*, 1993, **98**, 5648–5652.
26 J. R. Lakowicz, *Principles of fluorescence spectroscopy*, Springer Science+Business Media LLC, Boston, MA, 3rd edn, 2006.
27 I. B. Berlman, *Handbook of fluorescence spectra of aromatic molecules*, Academic Press, New York, 2nd edn, 1971.
28 M. Kasha, *Discuss. Faraday Soc.*, 1950, **9**, 14.
29 (*a*) A. Mishra, K. Sharma, C. E. Johnson, E. A. Fosu, J. Schwarz, O. Prakash, A. K. Gupta, P. Huang, F. Lindgren, L. Häggström, J. Bendix, E. Jakubikova, R. Lomoth and K. Wärnmark, *Chemistry*, 2025, **31**(47), e01985; (*b*) C. E. Johnson, J. Schwarz, M. Deegbey, O. Prakash, K. Sharma, P. Huang, T. Ericsson, L. Häggström, J. Bendix, A. K. Gupta, E. Jakubikova, K. Wärnmark and R. Lomoth, *Chem. Sci.*, 2023, **14**, 10129–10139.
30 W. McCall, T. M. Christy, D. A. Pipp, B. Jaster, J. White, J. Goodrich, J. Fontana and S. Doxtader, *Environ. Earth Sci.*, 2018, **77**, 374.
31 C. B. Roberts, J. F. Brennecke and J. E. Chateauneuf, *J. Chem. Soc., Chem. Commun.*, 1993, 868–869.
32 J. R. Schoonover, D. M. Dattelbaum, A. Malko, V. I. Klimov, T. J. Meyer, D. J. Styers-Barnett, E. Z. Gannon, J. C. Granger, W. S. Aldridge and J. M. Papanikolas, *J. Phys. Chem. A*, 2005, **109**, 2472–2475.
33 B. Lang, S. Mosquera-Vázquez, D. Lovy, P. Sherin, V. Markovic and E. Vauthey, *Rev. Sci. Instrum.*, 2013, **84**, 73107.
34 J. K. S. Wan, *Res. Chem. Intermed.*, 1990, **13**, 193.
35 R. Livingston and D. W. Tanner, *Trans. Faraday Soc.*, 1958, **54**, 765.